

Assembling PNIPAM-Capped Gold Nanoparticles in Aqueous Solutions

Binay P. Nayak,[†] Hyeong Jin Kim,[†] Srikanth Nayak,^{†,||} Wenjie Wang,[‡] Wei Bu,[¶]
Surya K. Mallapragada,^{*,†} and David Vaknin^{*,§}

[†]*Ames National Laboratory, and Department of Chemical and Biological Engineering, Iowa State University, Ames, Iowa 50011, United States*

[‡]*Division of Materials Sciences and Engineering, Ames National Laboratory, U.S. DOE, Ames, Iowa 50011, United States*

[¶]*NSF's ChemMatCARS, Pritzker School of Molecular Engineering, University of Chicago, Chicago, Illinois 60637, United States*

[§]*Ames National Laboratory, and Department of Physics and Astronomy, Iowa State University, Ames, Iowa 50011, United States*

^{||}*Current address: Chemical Sciences and Engineering Division, Argonne National Laboratory, Lemont, Illinois 60439, United States*

E-mail: suryakm@iastate.edu; vaknin@ameslab.gov

Abstract

Employing small angle X-ray scattering (SAXS), we explore the conditions under which assembly of gold nanoparticles (AuNPs) grafted with the thermo-sensitive polymer Poly(*N*-isopropylacrylamide) (PNIPAM) emerges. We find that short-range order assembly emerges by combining the addition of electrolytes or polyelectrolytes with raising the temperature of the suspensions above the lower-critical solution temperature (LCST) of PNIPAM. Our results show that the longer the PNIPAM chain is, the better organization in the assembled clusters. Interestingly, without added electrolytes, there is no evidence of AuNPs assembly as a function of temperature, although untethered PNIPAM is known to undergo a coil-to-globule transition above its LCST. This study demonstrates another approach to assembling potential thermo-sensitive nanostructures for devices by leveraging the unique properties of PNIPAM.

Main

Poly(*N*-isopropylacrylamide) (PNIPAM) is an amphiphilic polymer comprising an alkyl-chain back-bone decorated with amide-isopropyl side groups. The amide side groups, common to protein chains, render hydrophilic properties to the polymer. PNIPAM has attracted attention across disciplines due to its unique thermally responsive behavior. The polymer exhibits a lower critical solution temperature (LCST) at ~ 32 °C,^{1,2} above which the chains expel water and undergo contraction to a cascade of globular conformations.³ It has been established that the LCST phase transition is reversible. In addition, small angle neutron scattering of PNIPAM suspensions shows evidence of reversible assembly of the globular structures.⁴ This unique property has been widely explored for drug delivery,^{5,6} bio-sensors,^{7,8} smart layers,^{9,10} and microactuator.^{11,12} The thermal properties of PNIPAM make it a suitable candidate for surface modifications of nanoparticles (NPs) to create stimuli-responsive self-assembly and crystallization.^{13,14}

Recently, PNIPAM has been synthesized with a thiol end-group, making it suitable for grafting metallic NPs, particularly gold and silver.¹⁵ Indeed, temperature-induced assembly of PNIPAM grafted nanoparticles has been observed above the LCST by varying salinity, pH, and by photoexcitation.^{16–20} Various dynamic light scattering (DLS) and ultraviolet-visible (UV-Vis) studies have shown that the hydrodynamic diameter (D_H) of PNIPAM grafted AuNPs in pure water decreases marginally above the LCST. However, upon adding sodium chloride to the solutions, aggregation emerges above the LCST.^{16,17,19,21–23} Using block copolymer, poly(ethylene glycol)-*b*-poly(*N*-isopropylacrylamide) to graft AuNPs, it has been shown that self-assembly into one-dimensional (1D) or two-dimensional (2D) structures in salt solutions can be induced by raising the temperature above the LCST.²⁴ The same study emphasizes the significance of adding charged molecules to the grafted NP suspensions to achieve assembly. Other studies of grafted AuNPs with PNIPAM have been shown to exhibit assembly in two dimensions at air/liquid interfaces.^{25–27} Although thermal effects have not been reported to achieve assembly, the polymer tends to respond to the salinity of the suspension in a similar manner as has been observed for poly-ethylene glycol (PEG) grafted AuNPs.^{28,29}

Here, we extend these 2D studies to the three-dimensional (3D) bulk self-assembly and ordering by monitoring the combined effect of salinity and temperature. DLS studies have indicated assembly upon a variable salinity and temperature combination.²⁴ We employ *in-situ* synchrotron-based small angle scattering (SAXS) technique to determine the nature of the assembly upon adding electrolytes and varying the temperature.³⁰ As for electrolytes, we use salts such as potassium carbonate (K_2CO_3), sodium chloride (NaCl), or long-chain positively charged poly-electrolyte Poly(diallyldimethylammonium chloride) (PDAC). PDAC has been shown to induce 2D crystallization of sodium dodecyl sulfide at the air/liquid interface, making it a potential electrolyte to facilitate assembly.³¹ We also examine the effect of

grafted PNIPAM molecular weight (~ 3 vs. 6 kDa) on the characteristics of the assembly.

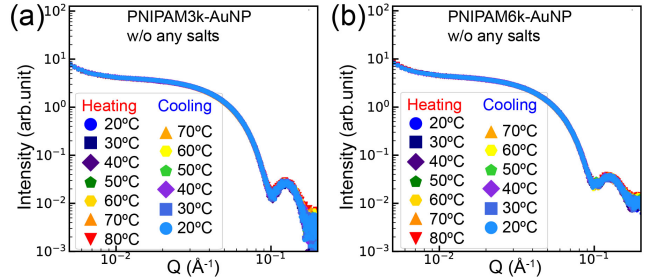


Figure 1: SAXS data for (a) PNIPAM3k-AuNPs (10 nm core) and (b) PNIPAM6k-AuNPs (10 nm core) in water (i.e., without any electrolytes) at various temperatures as indicated. The normalized intensity profiles $S(Q)$ are shown in SI Figure S7 and prove that no assembly occurs upon raising the temperature.

Raising the temperature above the LCST, without adding any electrolytes, the PNIPAM-AuNPs remain dispersed in the suspensions. Figure 1 shows SAXS patterns obtained from PNIPAM-AuNPs without salts at various temperatures (heating and cooling cycles). The pattern for PNIPAM3k-AuNPs in (a) and PNIPAM6k-AuNPs (b), up to 80 °C consists of the form factor of the core AuNPs (See Figure S5). We note that the SAXS intensities are dominated by the form factor of the AuNP core with little contribution from the PNIPAM corona. These results do not provide clear evidence for conformational change above the LCST of PNIPAM-AuNPs. We conclude that the particles remain dispersed in the suspensions even above the LCST. This is consistent with the globular shrinking conformation above the LCST,³ where the polymer likely exposes its hydrophilic moieties to the aqueous medium. The absence of assembly in pure water above LCST can be rationalized by the repulsion between the hydrophilic (dipolar) moieties.^{17,23} The lack of scattering from the PNIPAM corona in aqueous suspensions is due to a negligible electron-density (ED) contrast between the suspension (water) and the organic polymer. As a result, one cannot infer from SAXS measurements moderate changes in the conformations of the polymer in the corona. The normalized intensity profiles $S(Q)$ are shown in Figure S7 of the SI, confirming well-dispersed grafted AuNPs at all measured temperatures. More details on the form factor, the core size of AuNPs,

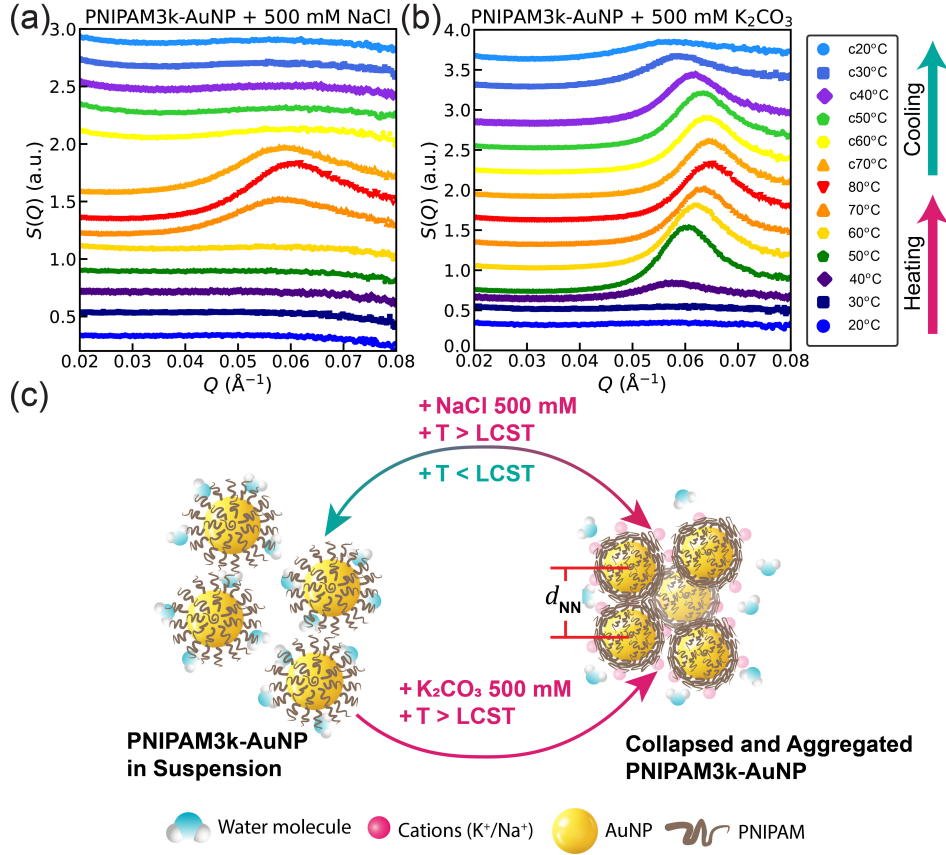


Figure 2: Normalized intensity $S(Q)$ data for PNIPAM3k-AuNPs with (a) 500 mM NaCl, (b) 500 mM K_2CO_3 at various temperatures, as indicated, showing the emergence of broad interference peak at $Q \simeq 0.055 \text{ \AA}^{-1}$. Such a lone broad peak indicates amorphous aggregation of particles with a characteristic nearest neighbor distance $d_{NN} \sim 11.5 \text{ nm}$. (c) Schematic illustration of the transition from dispersed nanoparticles to aggregates as the temperature is raised above the LCST in the presence of salts. The depicted aggregates show the particles with collapsed PNIPAM corona inferred from the value of d_{NN} , which is close to the NP core diameter.

and the size distribution of the citrate-stabilized AuNPs are provided in the SI.

Raising the temperature above the LCST in the presence of salts induces aggregation of PNIPAM3k-AuNPs. At low salt concentrations (below 50 mM of NaCl or K_2CO_3), the SAXS data show that the particles are dispersed in the suspensions even at elevated temperatures above the LCST, as shown in Figure S9. Figure 2 shows SAXS $S(Q)$ patterns of PNIPAM3k-AuNPs at 500 mM (a) NaCl and (b) K_2CO_3 . Adding K_2CO_3 or NaCl to the solution at room temperature yields SAXS patterns that are similar to those shown in Figure 1 (i.e., without salts). However, heating the same salinated suspensions above $\sim 40 \text{ }^\circ\text{C}$ gives rise to the emergence of a prominent peak around $Q_0 = 0.06 \text{ \AA}^{-1}$, which gradually shifts to a higher Q value upon further increase in temperature. This stand-alone peak indicates random aggregation of NPs with a characteristic nearest-neighbor

(NN) distance (d_{NN}), indicating liquid-like order. The characteristic $d_{NN} \simeq \frac{2\pi}{Q_0} \simeq 10.4 \text{ nm}$ is slightly larger than the diameter of the core AuNPs ($D_{\text{Core}} = 8.7 \text{ nm}$, see Figure S5). Such a small d_{NN} close to the D_{Core} suggests that the polymer is likely collapsed to its densely packed state (void of water) onto the NP surface. In the SI, we determine an upper limit to the grafting density, assuming such a densely packed collapsed corona. Furthermore, the shift in peak position to higher Q values as the temperature increases indicates smaller d_{NN} and further collapse of the grafted PNIPAM corona consistent with the globular behavior of pure PNIPAM in aqueous solutions.³ We define collapse as a densely-packed dry polymer with its hydrophilic moieties exposed to the aqueous medium.²⁶ We hypothesize that the observed aggregation is induced by the presence of the cations and anions that lead to attractive interaction among the NPs. We argue that the ions

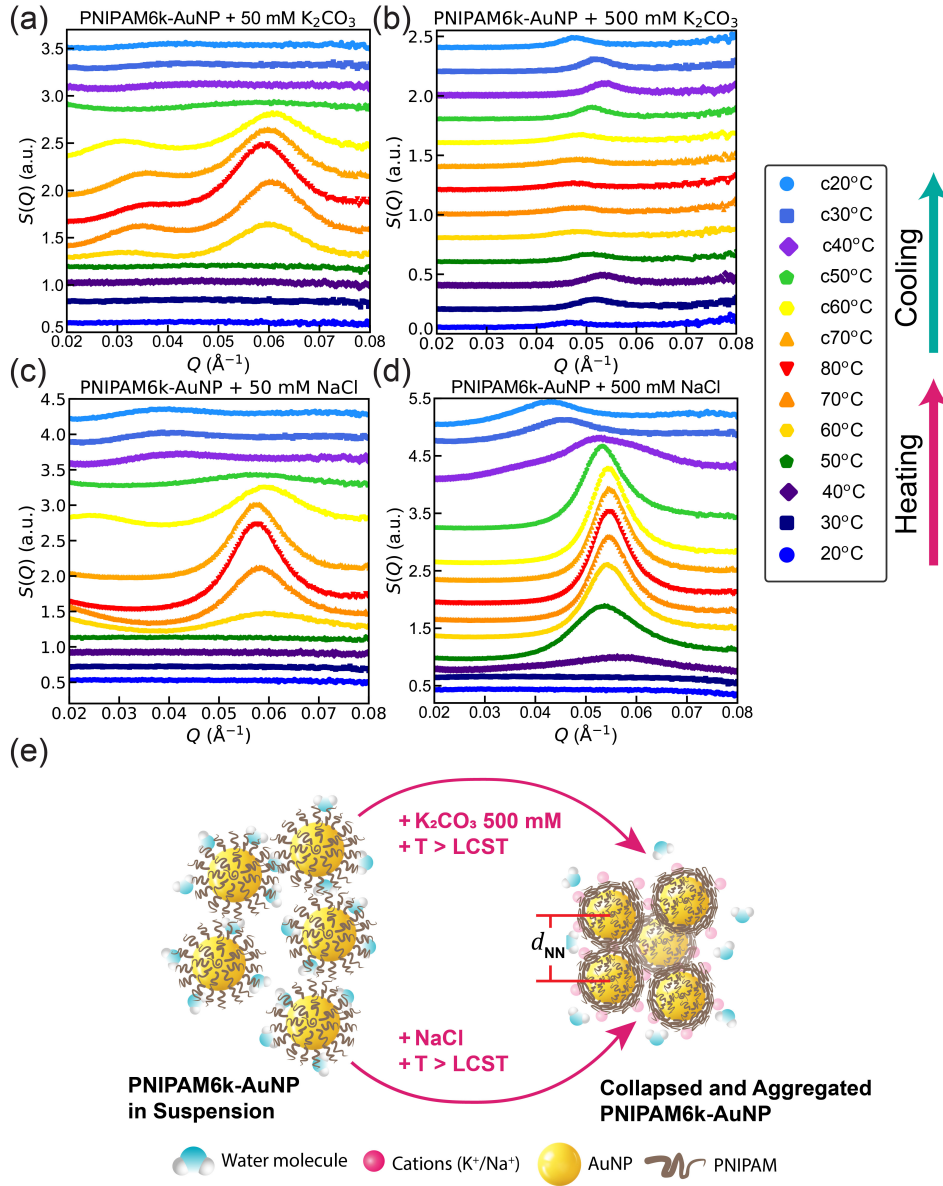


Figure 3: Normalized intensity $S(Q)$ patterns for PNIPAM6k-AuNPs with (a) 50 mM K_2CO_3 , showing two broad diffraction peaks. In the SI (Figure S11), we show that the diffraction pattern is best-describing clusters with diamond-like motifs. Our conclusion is based on examining various other structural scenarios. (b) 500 mM K_2CO_3 shows a single weak peak corresponding to a $d_{\text{NN}} \simeq 12.5$ nm. It is also likely that at this concentration, precipitation occurs. (c) 50 mM NaCl, (d) 500 mM NaCl at various temperatures as indicated, showing a single peak as described in Figure 2. (e) Schematic illustrations of the assembly development from dispersed NPs to aggregated are presented. Note that in this case, the assembly process is irreversible.

decorate different parts of the polymer corona, leading to weak mutual binding. As a result, upon cooling the suspension from 80 °C to room temperature, the NPs seem to re-disperse in the suspensions, as the hydrophilic moieties are less exposed. The evidence for re-dispersed clusters is that the prominent peak at Q_0 broadens significantly and almost diminishes upon cooling, indicative of the reversible nature of the collapsed state. We note that the addition of K_2CO_3 leads to a sharper $S(Q)$ peak and at larger Q values compared to those obtained by

adding NaCl. This indicates that K_2CO_3 , at elevated temperatures, leads to higher densely packed polymer corona with more well-defined d_{NN} . Our analysis of the diffraction patterns yields peak positions and line widths as shown in Table S1. The line widths indicate that the correlation lengths in the ordered states for 500 mM K_2CO_3 and NaCl is on the order of ~ 90 and 60 nm, respectively (i.e., 8-5 correlated NN). In addition, the aggregation is not fully reversible in the presence of K_2CO_3 . We note that K_2CO_3 , unlike NaCl, releases a divalent an-

ion, i.e., CO_3^{-2} whereas NaCl has a monovalent anion. More importantly, K_2CO_3 affects the pH (increases the alkalinity) of the suspension. We hypothesize that these differences affect the behavior of the assembled particles. In fact, assembling PEG-grafted AuNPs shows notable assembly differences between NaCl and K_2CO_3 in addition to the suspensions.³²

Similar to PNIPAM3k-AuNPs, the addition of NaCl or K_2CO_3 to the suspensions of PNIPAM6k-AuNP has little effect below the LCST, even at concentrations of salt as high as 500 mM. A more noticeable effect of salt addition with temperature for PNIPAM6k-AuNPs is apparent at 50 mM K_2CO_3 above the LCST. As shown in Figure 3(a), two broad peaks ($Q_1 \sim 0.035$ and $Q_2 \sim 0.06 \text{ \AA}^{-1}$) appear upon heating the suspension above 50 °C. Although it is difficult to assign a definite structure from such a limited diffraction pattern, we rationalize our proposed structure based on the behavior of the polymer at different temperatures. In particular, we assume that above the LCST, the polymer corona collapses onto the core of the AuNP. This constraint limits the possible packings of assembled nanoparticles. In the SI, we examine various structural scenarios and conclude that the likely packing has diamond-like motifs,³³ albeit at very short-range order. The correlation length in the ordered states is of the order of 2-3 unit cells. Figure 4(a) shows $S(Q)$ profile of PNIPAM6k-AuNP10 at 50 mM K_2CO_3 and 80 °C, fitted to a relaxed diamond-like structure using the first three Bragg reflection peaks. Our model allows small variations in the lattice positions of the AuNPs. The model system accounts for lattice positions with which we calculate the structure factor. A similar diffraction pattern associated with diamond-like structures has been reported for assembled binary Au and Ag NP systems.³³ This interpretation yields a $d_{\text{NN}}(\frac{3\pi}{2Q_{111}}) \simeq 13.1 \text{ nm}$, which is consistent with the grafting density and the fact that the polymer is densely packed (collapsed). See Figure S11 and further discussions in the SI.

At a high concentration of K_2CO_3 (500 mM), the diffraction pattern consists of a single weak peak at $Q \sim 0.05 \text{ \AA}^{-1}$ as shown in Figure 3(b).

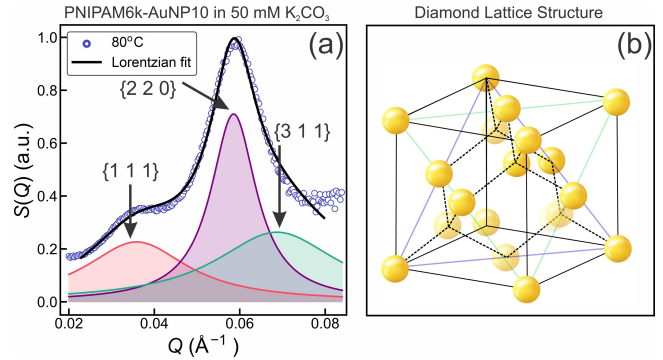


Figure 4: (a) $S(Q)$ profile of PNIPAM6k-AuNP10 at 50 mM K_2CO_3 and 80 °C, fitted to a relaxed diamond-like structure using the first three Bragg reflection peaks. The model system accounts for lattice positions with which we calculate the structure factor. The shaded peaks show the contribution of each Bragg reflection to the fitted data. (b) Schematic of a diamond-cubic lattice where the golden spheres represent the collapsed PNIPAM-AuNPs.

As mentioned above, a single peak can only provide minimal information on the characteristic length scale of d_{NN} ; in this case, $d_{\text{NN}} \sim 12.5 \text{ nm}$. It is also possible that better quality crystals are formed and precipitate out of the suspension and, therefore, are not detected in our bulk solution SAXS measurements. In the SI, we show the assembly of PNIPAM6k-AuNP at the liquid/vapor interface in the presence of 100 mM K_2CO_3 . The 2D diffraction pattern (grazing-incidence small-angle X-ray scattering; GISAXS) in Figure S12 shows two broad diffraction peaks similar to those observed in the bulk SAXS, however, at slightly smaller Q values. This suggests that the packing at the liquid/vapor interface is similar to that in bulk, and the d_{NN} is slightly larger at the surface. This is expected as the GISAXS measurements are performed below the LCST. We also note that the threshold for ordering in 2D is less strict than in 3D. In 2D, it is sufficient to achieve surface assembly with increased salinity even below the LCST at room temperature. By contrast, 3D assembly is induced by the combination of salinity and elevated temperature. More evidence on the 2D assembly of PNIPAM6k-AuNPs is established with X-ray reflectivity measurements and their analysis as shown in Figure S12.

The addition of 50 and 500 mM NaCl to the PNIPAM6k-AuNPs suspension has a similar effect on the assembly. As shown in Figure 3 (c) and (d), the addition of salt has little effect be-

low the LCST. Upon heating, a single peak at about $Q \sim 0.055 \text{ \AA}^{-1}$ emerges and grows in intensity up to 80 °C and decreases in intensity and shifts to lower Q values (at 20 °C the peak is centered around $Q \sim 0.045 \text{ \AA}^{-1}$) demonstrating the reversibility of collapsed state. The observed peak above the LCST is associated with a $d_{\text{NN}} \sim 11.5 \text{ nm}$ and below the LCST $d_{\text{NN}} \sim 14.1 \text{ nm}$ consistent with the globular shrinking of the PNIPAM above the LCST and expanding below it. For NaCl at 50 and 500 mM, we find that the Correlation length is in order of 50 and 100 nm, respectively.

To generalize the effect of assembly using polyelectrolytes, we use PDAC as an additive to the suspension to induce assembly. Figure S6 (a) shows the normalized intensity vs Q for the grafted AuNPs in the presence of $\sim 1 \text{ wt} \%$ PDAC. Unlike the simple salts, the polyelectrolyte induces assembly below the LCST (See Figure S6). At room temperature, the SAXS pattern has a broad peak at about $Q_0 = 0.04 \text{ \AA}^{-1}$ which, upon raising the temperature above 35 °C, shifts to $Q_0 = 0.053 \text{ \AA}^{-1}$. As discussed above, the single peak indicates $d_{\text{NN}} = 11.8 \text{ nm}$, consistent with a collapsed PNIPAM corona. More details are provided in the SI.

In summary, we have successfully grafted AuNPs with PNIPAM to achieve temperature-induced assembly and ordering of the NPs. Using synchrotron-based SAXS, we find that temperature has little effect on the nanoparticle assembly in the absence of salts. In fact, the SAXS provides clear evidence that in the absence of salts, the grafted AuNPs are well dispersed in the suspension, even upon heating above LCST. This may be due to the fact that above the LCST, PNIPAM exposes its hydrophilic moieties in the aqueous medium and becomes more soluble. By adding electrolytes (such as K_2CO_3 , NaCl, or long chain polyelectrolyte PDAC) to the solution, aggregation emerges. We hypothesize that the mutual attractive interaction among NPs is due to the accumulation of cations and anions on the surfaces of the polymer corona. These interactions lead only to very short-range order assembly such that the SAXS diffraction patterns resemble those of liquids. Our results suggest that

the longer the PNIPAM chain, the better organization in the assembled clusters.

Supporting Information

The Supporting Information is available free of charge on the ACS Publications website at DOI: xxxxx/yyyyy.

Experimental section; Additional DLS data; Additional SAXS data; Structural analysis; 2D XRR and GISAXS data; Calculation of grafting density; Calculation for molarity

Acknowledgements

The authors thank Jack Lawrence for help in grafting PNIPAM to gold nanoparticles. The authors acknowledge the infrastructure and support provided by the staff at beamline 12-ID-B, Advanced Photon Source (APS), Argonne National Laboratory. The research was financially supported by the U.S. Department of Energy (U.S. DOE), Office of Basic Energy Sciences, Division of Materials Sciences and Engineering. Iowa State University operates Ames National Laboratory for the U.S. DOE under Contract DE-AC02-07CH11358. Part of this research used NSF's ChemMatCARS Sector 15. NSF's ChemMatCARS Sector 15 is supported by the Divisions of Chemistry (CHE) and Materials Research (DMR), National Science Foundation, under grant number NSF/CHE-1834750. The use of the Advanced Photon Source, an Office of Science User Facility operated for the U.S. Department of Energy (DOE) Office of Science by Argonne National Laboratory, was supported by the U.S. DOE under Contract No. DE-AC02-06CH11357.

Author contributions

WW, DV, and SM conceived and supervised the project. HK, SN, DV, and WW designed, conducted the experiments and analyzed the data. BN, HK, WW, and DV wrote the manuscript. WB supported in X-ray scattering experiments, data acquisition, and data processing at NSF's

ChemMatCARS. SM, DV, and WW secured the funding for the project. All co-authors read and reviewed the manuscript.

References

- (1) Zhulina, E.; Borisov, O.; Pryamitsyn, V. A.; Birshtein, T. Coil-globule type transitions in polymers. 1. Collapse of layers of grafted polymer chains. *Macromolecules* **1991**, *24*, 140–149.
- (2) Heskins, M.; Guillet, J. E. Solution properties of poly (N-isopropylacrylamide). *Journal of Macromolecular Science—Chemistry* **1968**, *2*, 1441–1455.
- (3) Wu, C.; Wang, X. Globule-to-coil transition of a single homopolymer chain in solution. *Physical review letters* **1998**, *80*, 4092.
- (4) Filippov, S. K.; Bogomolova, A.; Kaberov, L.; Velychkivska, N.; Starovoytova, L.; Cernochova, Z.; Rogers, S. E.; Lau, W. M.; Khutoryanskiy, V. V.; Cook, M. T. Internal nanoparticle structure of temperature-responsive self-assembled PNIPAM-b-PEG-b-PNIPAM triblock copolymers in aqueous solutions: NMR, SANS, and light scattering studies. *Langmuir* **2016**, *32*, 5314–5323.
- (5) Xiong, W.; Wang, W.; Wang, Y.; Zhao, Y.; Chen, H.; Xu, H.; Yang, X. Dual temperature/pH-sensitive drug delivery of poly (N-isopropylacrylamide-co-acrylic acid) nanogels conjugated with doxorubicin for potential application in tumor hyperthermia therapy. *Colloids and Surfaces B: Biointerfaces* **2011**, *84*, 447–453.
- (6) Cao, M.; Wang, Y.; Hu, X.; Gong, H.; Li, R.; Cox, H.; Zhang, J.; Waigh, T. A.; Xu, H.; Lu, J. R. Reversible thermoresponsive peptide–PNIPAM hydrogels for controlled drug delivery. *Biomacromolecules* **2019**, *20*, 3601–3610.
- (7) Ma, H.; Zou, Y.; Zhang, S.; Liu, L.; Yu, J.; Fan, Y. Nanochitin and poly (N-isopropylacrylamide) interpenetrating network hydrogels for temperature sensor applications. *Carbohydrate Polymers* **2022**, *291*, 119544.
- (8) Guan, Y.; Zhang, Y. PNIPAM microgels for biomedical applications: from dispersed particles to 3D assemblies. *Soft Matter* **2011**, *7*, 6375–6384.
- (9) Wang, W.; Metwalli, E.; Perlich, J.; Papadakis, C.; Cubitt, R.; Müller-Buschbaum, P. Cyclic switching of water storage in thin block copolymer films containing poly (N-isopropylacrylamide). *Macromolecules* **2009**, *42*, 9041–9051.
- (10) Rotzetter, A. C.; Schumacher, C. M.; Bubenhofer, S. B.; Grass, R. N.; Gerber, L. C.; Zeltner, M.; Stark, W. J. Thermoresponsive polymer induced sweating surfaces as an efficient way to passively cool buildings. *Advanced materials* **2012**, *24*, 5352–5356.
- (11) Zhang, X.; Pint, C. L.; Lee, M. H.; Schubert, B. E.; Jamshidi, A.; Takei, K.; Ko, H.; Gillies, A.; Bardhan, R.; Urban, J. J.; Wu, M.; Fearing, R.; Javey, A. Optically-and thermally-responsive programmable materials based on carbon nanotube-hydrogel polymer composites. *Nano letters* **2011**, *11*, 3239–3244.
- (12) Tu, Y.; Peng, F.; Sui, X.; Men, Y.; White, P. B.; van Hest, J. C.; Wilson, D. A. Self-propelled supramolecular nanomotors with temperature-responsive speed regulation. *Nature chemistry* **2017**, *9*, 480–486.
- (13) Ding, T.; Valev, V. K.; Salmon, A. R.; Forman, C. J.; Smoukov, S. K.; Scherman, O. A.; Frenkel, D.; Baumberg, J. J. Light-induced actuating nanotransducers. *Proceedings of the National Academy of Sciences* **2016**, *113*, 5503–5507.
- (14) Cormier, S.; Ding, T.; Turek, V.; Baumberg, J. J. Dynamic-and light-switchable

- self-assembled plasmonic metafilms. *Advanced Optical Materials* **2018**, *6*, 1800208.
- (15) Li, C.; Wang, C.; Ji, Z.; Jiang, N.; Lin, W.; Li, D. Synthesis of thiol-terminated thermoresponsive polymers and their enhancement effect on optical limiting property of gold nanoparticles. *European Polymer Journal* **2019**, *113*, 404–410.
- (16) Gibson, M. I.; O’Reilly, R. K. To aggregate, or not to aggregate? considerations in the design and application of polymeric thermally-responsive nanoparticles. *Chemical society reviews* **2013**, *42*, 7204–7213.
- (17) Zhang, Z.; Maji, S.; Antunes, A. B. d. F.; De Rycke, R.; Zhang, Q.; Hoogenboom, R.; De Geest, B. G. Salt plays a pivotal role in the temperature-responsive aggregation and layer-by-layer assembly of polymer-decorated gold nanoparticles. *Chemistry of Materials* **2013**, *25*, 4297–4303.
- (18) Jones, S. T.; Walsh-Korb, Z.; Barrow, S. J.; Henderson, S. L.; del Barrio, J.; Scherman, O. A. The importance of excess poly (N-isopropylacrylamide) for the aggregation of poly (N-isopropylacrylamide)-coated gold nanoparticles. *ACS nano* **2016**, *10*, 3158–3165.
- (19) Maji, S.; Cesur, B.; Zhang, Z.; De Geest, B. G.; Hoogenboom, R. Poly (N-isopropylacrylamide) coated gold nanoparticles as colourimetric temperature and salt sensors. *Polymer Chemistry* **2016**, *7*, 1705–1710.
- (20) Li, B.; Smilgies, D.-M.; Price, A. D.; Huber, D. L.; Clem, P. G.; Fan, H. Poly (N-isopropylacrylamide) surfactant-functionalized responsive silver nanoparticles and superlattices. *ACS nano* **2014**, *8*, 4799–4804.
- (21) Yusa, S.-i.; Fukuda, K.; Yamamoto, T.; Iwasaki, Y.; Watanabe, A.; Akiyoshi, K.; Morishima, Y. Salt effect on the heat-induced association behavior of gold nanoparticles coated with poly (N-isopropylacrylamide) prepared via reversible addition-fragmentation chain transfer (RAFT) radical polymerization. *Langmuir* **2007**, *23*, 12842–12848.
- (22) Vasicek, T. W.; Jenkins, S. V.; Vaz, L.; Chen, J.; Stenzen, J. A. Thermoresponsive nanoparticle agglomeration/aggregation in salt solutions: Dependence on graft density. *Journal of colloid and interface science* **2017**, *506*, 338–345.
- (23) Turek, V. A.; Cormier, S.; Sierra-Martin, B.; Keyser, U. F.; Ding, T.; Baumberg, J. J. The Crucial Role of Charge in Thermoresponsive-Polymer-Assisted Reversible Dis/Assembly of Gold Nanoparticles. *Advanced Optical Materials* **2018**, *6*, 1701270.
- (24) Kim, G.-H.; Kim, M.; Hyun, J. K.; Park, S.-J. Directional Self-Assembly of Nanoparticles Coated with Thermoresponsive Block Copolymers and Charged Small Molecules. *ACS Macro Letters* **2023**, *12*, 986–992.
- (25) Wang, W.; Lawrence, J. J.; Bu, W.; Zhang, H.; Vaknin, D. Two-dimensional crystallization of poly (N-isopropylacrylamide)-capped gold nanoparticles. *Langmuir* **2018**, *34*, 8374–8378.
- (26) Minier, S.; Kim, H. J.; Zaugg, J.; Malapragada, S. K.; Vaknin, D.; Wang, W. Poly (N-isopropylacrylamide)-grafted gold nanoparticles at the vapor/water interface. *Journal of Colloid and Interface Science* **2021**, *585*, 312–319.
- (27) Londoño-Calderon, A.; Wang, W.; Lawrence, J. J.; Bu, W.; Vaknin, D.; Prozorov, T. Salt-Induced Liquid-Liquid Phase Separation and Interfacial Crystal Formation in Poly (N-isopropylacrylamide)-Capped Gold

Nanoparticles. *The Journal of Physical Chemistry C* **2021**, *125*, 5349–5362.

- (28) Zhang, H.; Wang, W.; Mallapragada, S.; Travesset, A.; Vaknin, D. Macroscopic and Tunable Nanoparticle Superlattices. *Nanoscale* **2017**, *9*, 164–171.
- (29) Kim, H. J.; Wang, W.; Mallapragada, S.; Travesset, A.; Vaknin, D. Nanoparticle Superlattices with Negative Thermal Expansion (NTE) Coefficients. *The Journal of Physical Chemistry C* **2021**, *125*, 10090–10095.
- (30) Nayak, S.; Horst, N.; Zhang, H.; Wang, W.; Mallapragada, S.; Travesset, A.; Vaknin, D. Interpolymer Complexation as a Strategy for Nanoparticle Assembly and Crystallization. *The Journal of Physical Chemistry C* **2019**, *123*, 836–840.
- (31) Vaknin, D.; Dahlke, S.; Travesset, A.; Nizri, G.; Magdassi, S. Induced crystallization of polyelectrolyte-surfactant complexes at the gas-water interface. *Physical review letters* **2004**, *93*, 218302.
- (32) Zhang, H.; Wang, W.; Mallapragada, S.; Travesset, A.; Vaknin, D. Ion-specific interfacial crystallization of polymer-grafted nanoparticles. *The Journal of Physical Chemistry C* **2017**, *121*, 15424–15429.
- (33) Kalsin, A. M.; Fialkowski, M.; Paszewski, M.; Smoukov, S. K.; Bishop, K. J.; Grzybowski, B. A. Electrostatic self-assembly of binary nanoparticle crystals with a diamond-like lattice. *science* **2006**, *312*, 420–424.

For Table of Contents Use Only

Assembling PNIPAM-Capped Gold Nanoparticles in Aqueous Solutions

Binay P. Nayak,[†] Hyeong Jin Kim,[†] Srikanth Nayak,^{†,||} Wenjie Wang,[‡] Wei Bu,[¶] Surya K. Mallapragada,^{*,†} and David Vaknin^{*,§}

[†]*Ames National Laboratory, and Department of Chemical and Biological Engineering, Iowa State University, Ames, Iowa 50011, United States*

[‡]*Division of Materials Sciences and Engineering, Ames National Laboratory, U.S. DOE, Ames, Iowa 50011, United States*

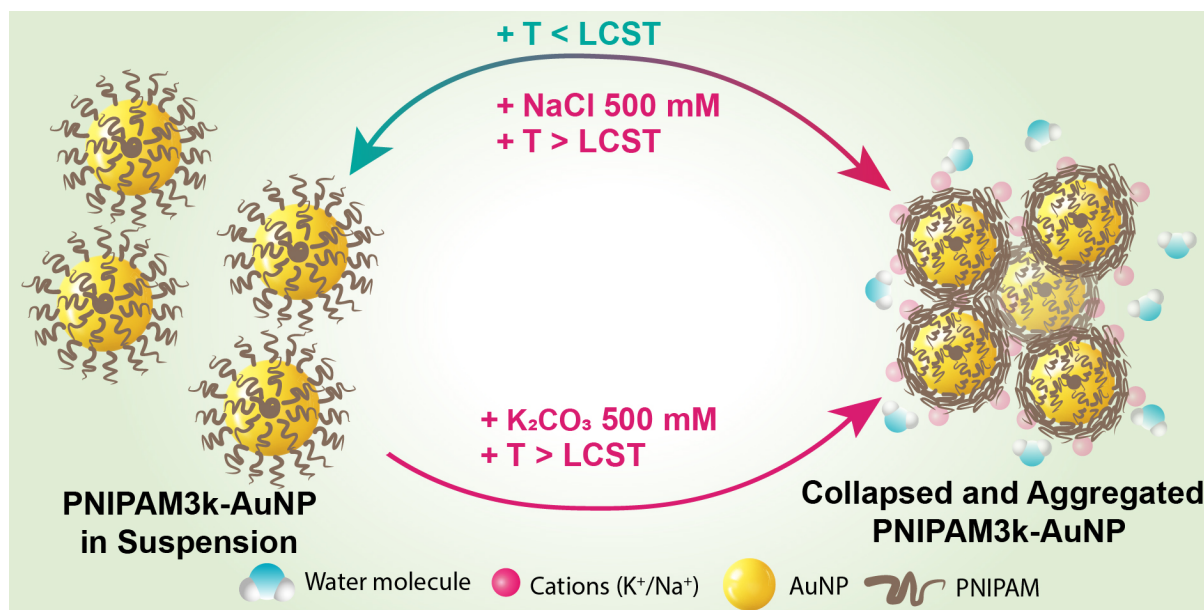
[¶]*NSF's ChemMatCARS, Pritzker School of Molecular Engineering, University of Chicago, Chicago, Illinois 60637, United States*

[§]*Ames National Laboratory, and Department of Physics and Astronomy, Iowa State University, Ames, Iowa 50011, United States*

^{||}*Current address: Chemical Sciences and Engineering Division, Argonne National Laboratory, Lemont, Illinois 60439, United States*

E-mail: suryakm@iastate.edu; vaknin@ameslab.gov

Table of Contents Graphic



Supporting information

Assembling PNIPAM-capped Gold Nanoparticles in Aqueous Solutions

Binay P. Nayak,[†] Hyeong Jin Kim,[†] Srikanth Nayak,^{†,||} Wenjie Wang,[‡] Wei Bu,[¶] Surya K. Mallapragada,^{*,†} and David Vaknin^{*,§}

[†]*Ames National Laboratory, and Department of Chemical and Biological Engineering, Iowa State University, Ames, Iowa 50011, United States*

[‡]*Division of Materials Sciences and Engineering, Ames National Laboratory, U.S. DOE, Ames, Iowa 50011, United States*

[¶]*NSF's ChemMatCARS, Pritzker School of Molecular Engineering, University of Chicago, Chicago, Illinois 60637, United States*

[§]*Ames National Laboratory, and Department of Physics and Astronomy, Iowa State University, Ames, Iowa 50011, United States*

^{||}*Current address: Chemical Sciences and Engineering Division, Argonne National Laboratory, Lemont, Illinois 60439, United States*

E-mail: suryakm@iastate.edu; vaknin@ameslab.gov

Experimental Section

Preparation of Materials

Citrate stabilized AuNPs suspensions of nominal core diameter ~ 10 nm have been purchased from Ted Pella Inc. Thiolated PNIPAM of molecular weights (MW) ~ 3 and ~ 6 kDa have been purchased from Sigma Aldrich. The AuNPs were functionalized with thiolated PNIPAM (SH-PNIPAM) by a ligand exchange protocol, as outlined below.^{26,28} Thiolated PNIPAM ligands are dissolved in 50% (v/v) ethanol solution and mixed with a calculated amount of AuNPs suspension (1:6000 AuNP to polymer ratio) continuously with a Roto-Shake Genie shaker (Scientific Industries, NY, USA) for at least 24 hours. The resulting PNIPAM-grafted AuNPs (PNIAPM-AuNPs) are then purified by centrifugation thrice at 20000 g for 1 hour to remove unbound ligands. Throughout the study, the term PNIAPM-AuNP is used generally to refer to PNIPAM-grafted AuNPs in general, while PNIAPM x -AuNP indicates the PNIAPM ligands with an MW of x grafted to AuNPs. For example, PNIAPM3k-AuNPs refer to AuNPs functionalized with 3 kDa MW of PNIPAM. The final concentration of the PNIPAM-grafted AuNPs is determined by measuring their absorbance using UV-vis spectroscopy (SpectraMax M3, Molecular Devices). For this study, the bare AuNPs are utilized at a concentration of approximately 9.46 nM, while the concentration of PNIPAM-AuNPs is adjusted to approximately 20 nM. DLS determines the percentage intensity distribution of the D_H of well-dispersed NPs in aqueous suspensions. The measurements and data processing have been conducted with a NanoZS90 and its associated software, Zetasizer (Malvern, U.K.). From Figure S1, it is evident that D_H increases upon grafting and scales with the length of the polymer. We find that $D_H \simeq 12.1(3)$, $25.1(3)$, $27.8(6)$ nm for bare surface AuNPs, PNIPAM3k-AuNPs, and PNIPAM6k-AuNPs, respectively. This increase in size confirms the successful grafting of PNIPAM. For the X-ray measurements, the grafted AuNPs were studied at various electrolyte solutions such as K_2CO_3 and NaCl (Fisher Scientific) and PDAC (MW = 100 - 200 kDa, Sigma Aldrich). Prior to the X-ray experimentation, high concentrations of electrolyte stock solutions were prepared, and a calculated amount from the stock solution (relatively smaller than the volume of AuNPs

suspension) was then mixed with the PNIPAM-AuNPs suspension and allowed to incubate for \sim 20 minutes.

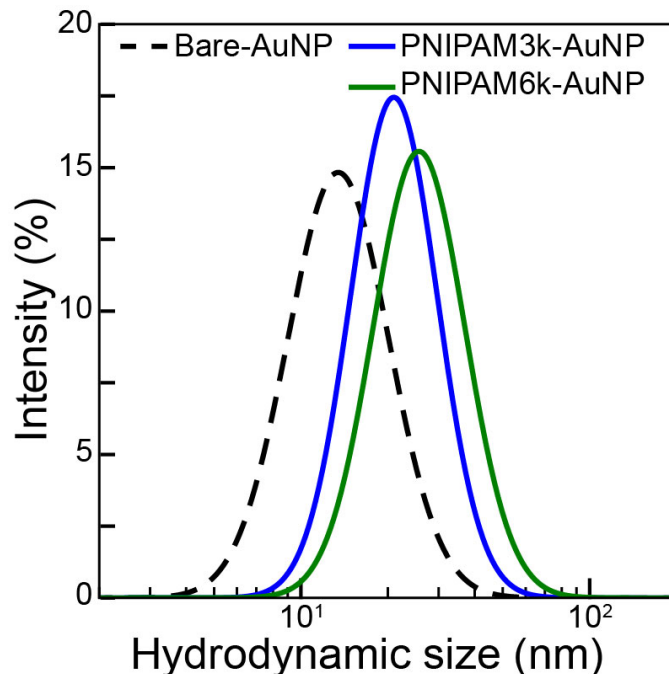


Figure S1: DLS intensity percentage versus hydrodynamic size distribution for aqueous suspensions of bare surface AuNPs (dashed-line), PNIPAM3k-AuNPs (blue-solid line), and PNIPAM6k-AuNPs (green solid-line) at room temperature. The increase in hydrodynamic size confirms PNIPAM grafting.

X-ray Experimental Setup

Synchrotron-based SAXS measurements were conducted at beamline 12-ID-B, Advanced Photon Source (APS), Argonne National Laboratory. The experiment is performed in transmission mode with an incident X-ray energy of 13.3 keV. After incubation, The PNIPAM-AuNPs suspensions with the desired solvent condition are transferred to a thin-walled quartz capillary (inner diameter of 2 mm). The temperature of the capillary loaded with the sample was elevated from 20 to 80 °C and subsequently cooled down to 20 °C at a 2 °C/min rate. SAXS measurements were collected at each 10 °C increment interval. Details of the experimental setup, measurements, and data analysis can be found elsewhere.^{29,30} The normalized intensity ($S(Q)$) is obtained by dividing the reduced intensity of the SAXS profile by the corresponding measured form factor of individual NPs.²⁹

Additional DLS data

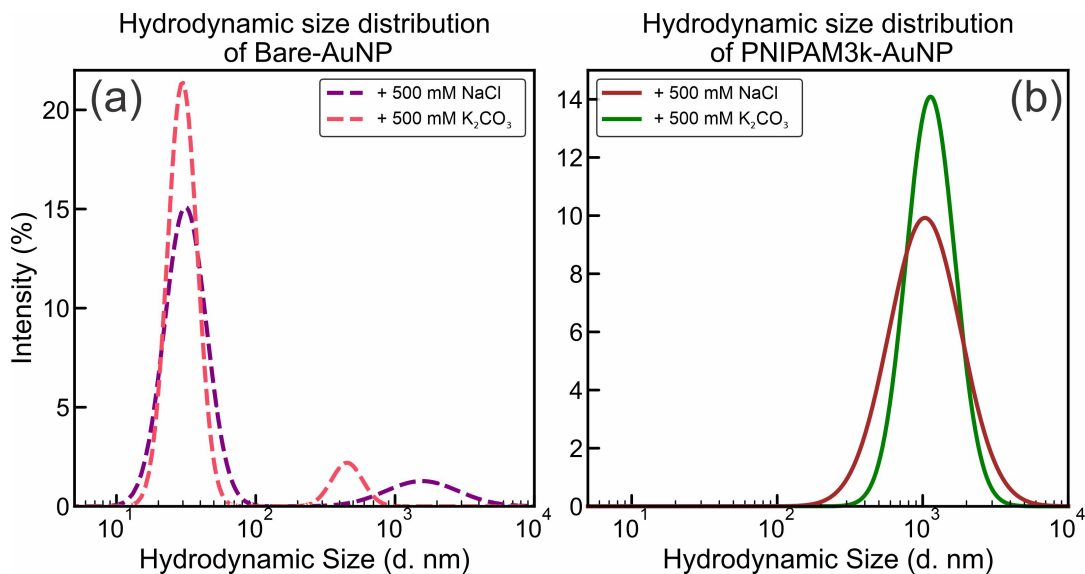


Figure S2: Hydrodynamic size distribution of (a) Bare AuNPs and (b) PNIPAM3k-AuNPs in the presence of 500 mM NaCl and K_2CO_3 at room-temperature as indicated. The bare AuNPs show minimal aggregation, whereas PNIPAM3k-AuNPs spontaneously aggregate at room temperature in the presence of salts.

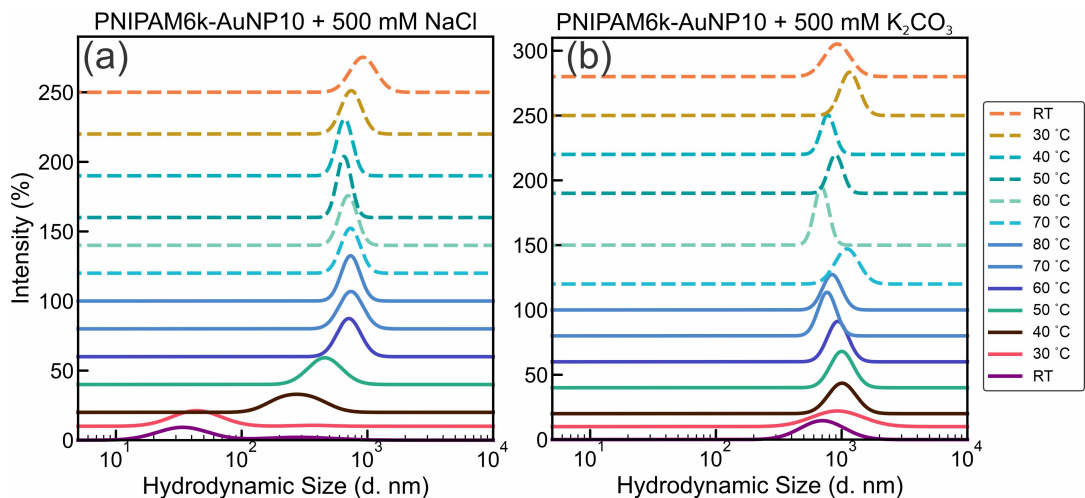


Figure S3: Hydrodynamic size distribution of PNIPAM6k-AuNPs in the presence of (a) 500 mM NaCl and (b) 500 mM K_2CO_3 at various temperatures as indicated.

Figure S2 shows DLS measurements for (a) bare AuNP and (b) PNIPAM3k-AuNP in the presence of 500 mM NaCl and K_2CO_3 at room-temperature as indicated. In the case of bare AuNPs, a tendency towards partial aggregation is observed under both salt conditions, although a significant proportion remains non-aggregated. In contrast, the PNIPAM3k-AuNPs exhibit a more pronounced response in the presence of salt, showing spontaneous aggregation when exposed to both NaCl and K_2CO_3 . The aggregates are considered as amorphous suggested by SAXS results. Figure S3 displays DLS measurements for PNIPAM6k-AuNP at (a) 500 mM NaCl and (b) 500 mM K_2CO_3 at various temperatures as indicated. At room temperature, PNIPAM6k-AuNP in 500 mM NaCl does not aggregate. However, increasing temperature above the LCST (to 40 °C) induces aggregation, which intensifies progressively with further temperature increase to 80 °C. This phenomenon is rationalized by the fact that PNIPAM corona collapses on the core, and binding is facilitated by the salts and thus promotes aggregation. When the temperature is reduced from 80 °C back to room temperature,

the PNIPAM6k-AuNPs remain aggregated. Interestingly, the aggregation size at room temperature after heating is larger than at 80 °C. This suggests that while the polymer corona may partially revert to its pre-heating expanded state, the nanoparticles remain as amorphous aggregates. In the presence of 500 mM K_2CO_3 , PNIPAM6k-AuNPs show spontaneous amorphous aggregation at room temperature. Intriguingly, upon gradually heating the suspension above the LCST, there is an observable decrease in aggregate size. This reduction is likely due to the shrinking of the PNIPAM corona (collapse) at elevated temperatures, reducing inter-particle distances. Cooling the suspension reverses this effect, leading to an increase in aggregate size.

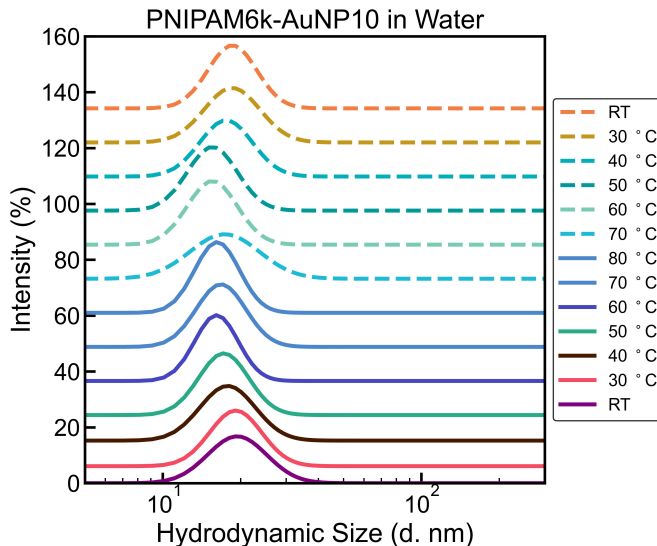


Figure S4: Hydrodynamic size distribution of PNIPAM6k-AuNPs in water at various temperatures as indicated. Without any electrolytes, PNIPAM6k-AuNPs do not aggregate upon heating the suspension.

As a control experiment, we examine the effect of temperature in the absence of salt on PNIPAM6k-AuNP; we conduct DLS measurements as shown in Figure S4. The message from this figure is that temperature by itself does not induce aggregation even above the LCST, and salt is needed to achieve aggregation, as discussed above. It is interesting to note that, as expected, raising the temperature changes the D_H to smaller values in accordance with the known behavior of the grafted polymer above the LCST.³ We note that the conditions under which we conduct in-situ SAXS measurements and DLS measurements are not the same, and some variations are expected.

Additional SAXS data

Figure S5 shows SAXS data from PNIPAM3k-AuNPs and PNIPAM6k-AuNPs in water (i.e., without any salts at room temperature) and their best-fit curves for the form factor profile of sphere (red solid lines). We note that due to the lack of electron density (ED) contrast between the polymer and the aqueous medium, the X-ray scattering from the grafted nanoparticle is dominated by the gold nanoparticle (AuNP) core.

Figure S6 shows normalized intensity profile $S(Q)$ profile obtained at different temperatures for PNIPAM6k-AuNPs at ~ 1 wt % of Poly(diallyl-dimethylammonium chloride) (PDAC). The polymer, unlike the salts, induces assembly at room temperature with a broad peak at $Q_0 = 0.04 \text{ \AA}^{-1}$ which, upon raising the temperature above 35 °C, shifts to $Q_0 = 0.053 \text{ \AA}^{-1}$. The process is irreversible; namely, the peak at room temperature remains pronounced.

Figure S7 shows normalized intensity profiles ($S(Q)$) from SAXS data for (a) PNIPAM3k-AuNP and (b) PNIPAM6k-AuNP in water under the temperature controls. The constant values of $S(Q)$ indicate dispersed NPs in the suspensions even above the LCST. Adding small amounts of salts 5

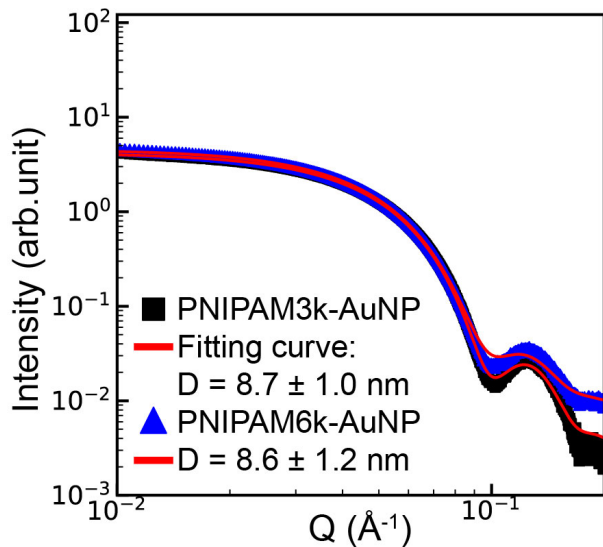


Figure S5: SAXS data for PNIPAM3k-AuNPs and PNIPAM6k-AuNPs in water (i.e., without any salts at room temperature) and their best-fit curves for the form factor profile of sphere (red solid lines).

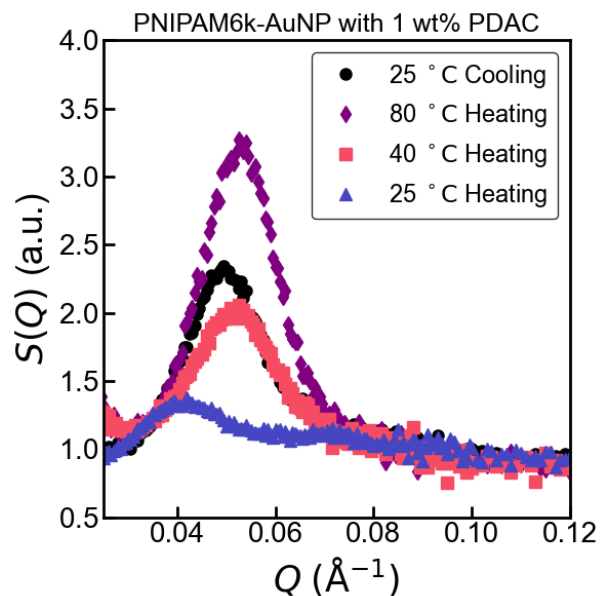


Figure S6: Normalized intensity profile $S(Q)$ profile obtained at different temperatures for PNIPAM6k-AuNPs at \sim 1wt % of Poly(diallyl-dimethylammonium chloride)

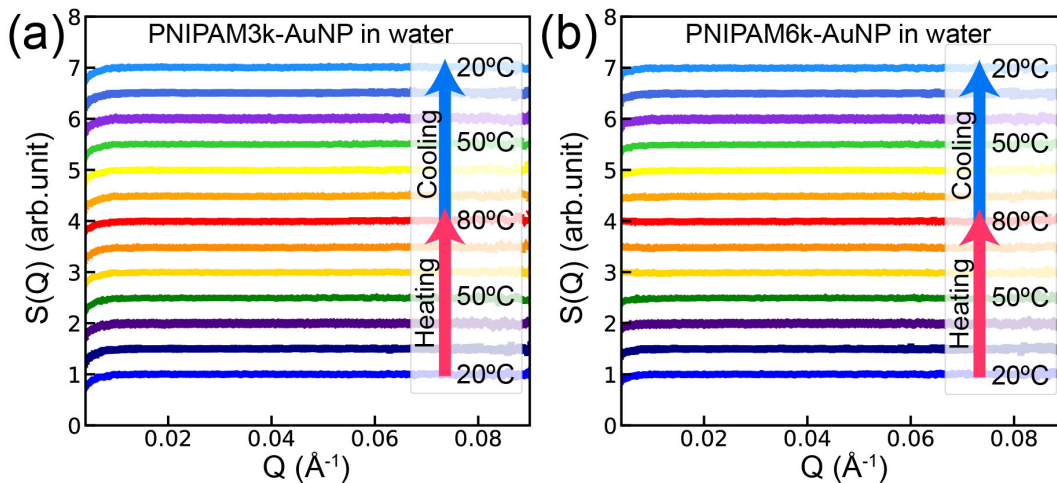


Figure S7: Normalized intensity profiles ($S(Q)$) from SAXS data for (a) PNIPAM3k-AuNP and (b) PNIPAM6k-AuNP in water under the temperature controls.

mM NaCl or K_2CO_3 (Figure S8) yields results that are practically the same as those in water. Note that for deductive purposes, we show the un-normalized scattering, namely the form factor of the NPs.

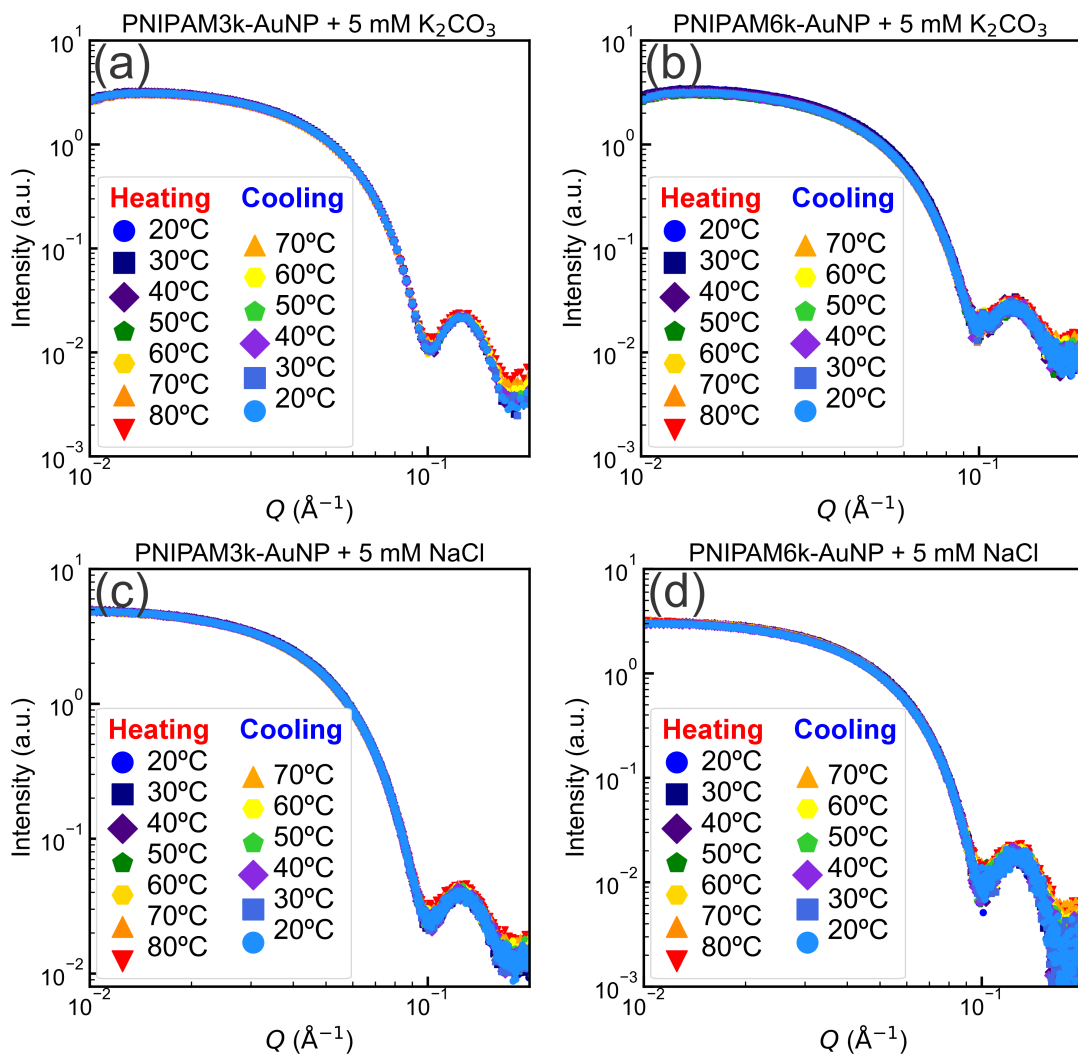


Figure S8: SAXS data for PNIPAM3k-AuNPs with (a) 5 mM of K_2CO_3 and (c) 5 mM NaCl and SAXS data for PNIPAM6k-AuNP with (b) 5 mM of K_2CO_3 and (d) 5 mM NaCl under the control of temperatures in the range of 20 – 80 °C heating and 80 – 20 °C cooling.

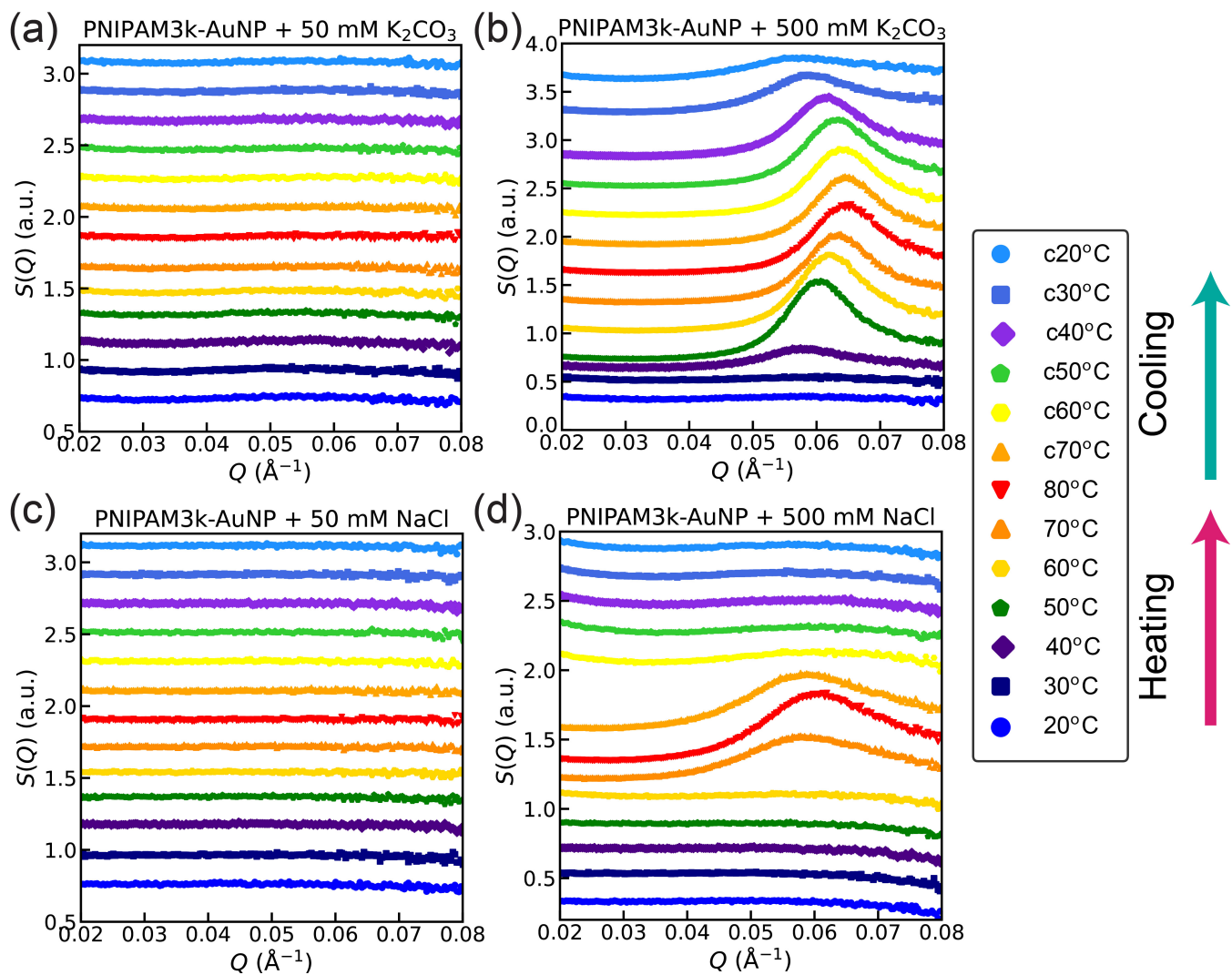


Figure S9: Normalized intensity profile $S(Q)$ profile obtained at different temperatures for PNIPAM3k-AuNPs at (a) 50 mM K_2CO_3 (b) 500 mM K_2CO_3 (c) 50 mM NaCl (d) 500 mM NaCl

Table S1: Summary of the nearest-neighbor distance and FWHM for different PNIPAM-AuNP assemblies induced under various electrolytes and temperatures as indicated. Temperature values labeled with the prefix “c” indicate that they were performed after cooling from 80 °C.

Name of PNIPAM-AuNP	Suspensions condition (°C)	Temperature	Q_{center} (\AA^{-1})	d_{NN}^{**} (nm)	FWHM [#] (\AA^{-1})
PNIPAM3k-AuNP	+ K ₂ CO ₃ 50 mM	<i>No structure observed at any temperature</i>			
	+ NaCl 50 mM	<i>No structure observed at any temperature</i>			
	+ K ₂ CO ₃ 500 mM	40	–	–	–
		50	0.0606 (1)	10.4 (1)	0.0062 (2)
		60	0.0624 (1)	10.1 (1)	0.0069 (1)
		70	0.0636 (1)	9.9 (1)	0.0067 (1)
		80	0.0649 (1)	9.7 (1)	0.0066 (1)
		c70	0.0648 (1)	9.7 (1)	0.0066 (1)
		c60	0.0643 (1)	9.8 (1)	0.0067 (1)
		c50	0.0635 (1)	9.9 (1)	0.0069 (1)
		c40	0.0619 (1)	10.2(1)	0.0075 (2)
		+ NaCl 500 mM	70	0.0596 (1)	10.6 (2)
	80		0.0611 (1)	10.3 (2)	0.0112 (2)
	c70		0.0596 (1)	10.6 (2)	0.0141 (2)
PNIPAM6k-AuNP	+ K ₂ CO ₃ 50 mM*	60	0.0314 (1)	15.0 (7)	0.0213 (7)
		70	0.0324 (1)	14.5 (4)	0.0212 (2)
		80	0.0359 (1)	13.1 (4)	0.0291 (1)
		c70	0.0364 (1)	12.9 (4)	0.0213 (2)
		c60	0.0317 (1)	14.9 (2)	0.0174 (2)
	+ NaCl 50 mM	60	0.0602 (1)	10.4 (1)	0.0218(4)
		70	0.0587 (1)	10.7 (1)	0.0095 (1)
		80	0.0577 (1)	10.9 (1)	0.0069 (1)
		c70	0.0578 (1)	10.9 (1)	0.0076 (1)
		c60	0.0597 (1)	10.5 (1)	0.0122 (2)
	+ K ₂ CO ₃ 500 mM	<i>No structure observed at any temperature</i>			
	+ NaCl 500 mM	40	–	–	–
		50	0.0541 (1)	11.6 (1)	0.0089 (1)
		60	0.0548 (1)	11.5 (1)	0.0057 (1)
70		0.0550 (1)	11.4 (1)	0.0048 (1)	
80		0.0549 (1)	11.4 (1)	0.0045 (1)	
c70		0.0550 (1)	11.4 (1)	0.0045 (1)	
c60		0.0548 (1)	11.5 (1)	0.0047 (1)	
c50		0.0537 (1)	11.7 (1)	0.0056 (1)	
c40		0.0541 (1)	11.6 (1)	0.0142 (6)	

* Only first peak corresponding to {111} plane of diamond cubic structure is reported. neighbor distance (d_{NN}) for diamond cubic lattice is $\frac{3\pi}{2Q_{111}}$. ** Q_{center} , d_{NN} and FWHM is reported for structures where applicable. # FWHM - Full Width at Half Maximum is estimated from the Lorentzian fitting function of the prominent peak.

Rationalization of Diamond-like structure for PNIPAM6k-AuNPs in 50 mM K_2CO_3 at 80 °C

Below, we examine a few model structures for SAXS measurements of PNIPAM6k-AuNPs in 50 mM K_2CO_3 at 80 °C and show that the more-likely structure is diamond-like, albeit at very short-range order (correlation-length is on the order of 1-2 unit cells). Figure S10 shows the SAXS data with expected intensities at the various Bragg reflections indicated and scaled as vertical dashed lines. See Table S2 for more detailed comparisons of relative calculated intensities. It is clear that for the BCC, FCC, and HCP model structures, the ratio between the first and higher-order peaks is greater than one and smaller than one for the diamond-like structure, as observed experimentally. We have, in fact, modeled these data sets using the four models, and the best fit is obtained with the diamond-like structure. Figure S11 shows fits the data at various temperatures, relaxing the calculated intensity $\pm 20\%$. The parameters are listed in Table S3. We note that our model is based on the similarity of our diffraction pattern with that observed in Ref.[33]. Although the assignment to a diamond structure should be taken with reservations, it is consistent with the conformation of PNIPAM at high temperatures; namely, the polymer is collapsed.

	(h, k, l)	Q_{hkl}/Q_0	m_{hkl}	I_{cal}
bcc	(1, 1, 0)	1	12	100.0
	(2, 0, 0)	$\sqrt{2}$	6	25.0
	(2, 1, 1)	$\sqrt{3}$	24	66.7
	(2, 2, 0)	2	12	25.0
	(3, 1, 0)	$\sqrt{5}$	24	40.0
	(2, 2, 2)	$\sqrt{6}$	8	11.1
	(3, 2, 1)	$\sqrt{7}$	48	57.1
fcc	(1, 1, 1)	1	8	100.0
	(2, 0, 0)	$\sqrt{4/3}$	6	56.3
	(2, 2, 0)	$\sqrt{8/3}$	12	56.3
	(3, 1, 1)	$\sqrt{11/3}$	24	81.8
	(2, 2, 2)	2	8	25.0
hexagonal	(1, 0, 0)	1	6	100.0
	(1, 1, 0)	$\sqrt{3}$	6	33.3
	(2, 0, 0)	2	6	25.0
	(2, 1, 0)	$\sqrt{7}$	12	28.6
	(3, 0, 0)	3	6	11.1
	(2, 2, 0)	$\sqrt{12}$	6	8.3
	(3, 1, 0)	$\sqrt{13}$	12	15.4
diamond	(1, 1, 1)	1	8	88.9
	(2, 2, 0)	$\sqrt{8/3}$	12	100.0
	(3, 1, 1)	$\sqrt{11/3}$	24	72.7
	(4, 0, 0)	$\sqrt{16/3}$	6	25.0

Table S2: Multiplicity (m_{hkl}) and relative observed intensity (I_{cal}) for different crystal structures.

The SAXS intensity I_{hkl} , i.e., integrated area for each indexed (h, k, l) peak, is mainly proportional to the corresponding multiplicity, m_{hkl} , multiplied by Lorentz factor that is proportional to $1/Q^2$, accounting for the observed intensity for powder diffraction. Here, we list m_{hkl} and relative calculated intensity, I_{cal} , that is proportional to m_{hkl}/Q^2 . Q_0 is the primary peak position, and the

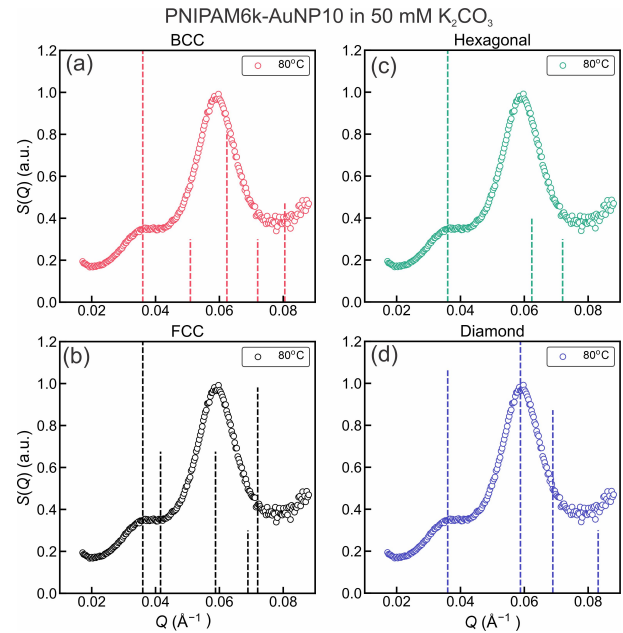


Figure S10: Calculated peak positions derived from $Q_0 = 0.0359 \text{ \AA}^{-1}$ (Table S1) for various lattice types are indicated by dashed lines. The height of each line corresponds to the relative calculated intensities for the respective lattice, as detailed in Table S2.

maximum peak intensity is scaled to 100. Within our Q range $0.01 - 0.08 \text{ \AA}^{-1}$, only the diamond structure is the most likely to account for the two apparent intensity maxima by three designated indexed peaks with comparable intensities.

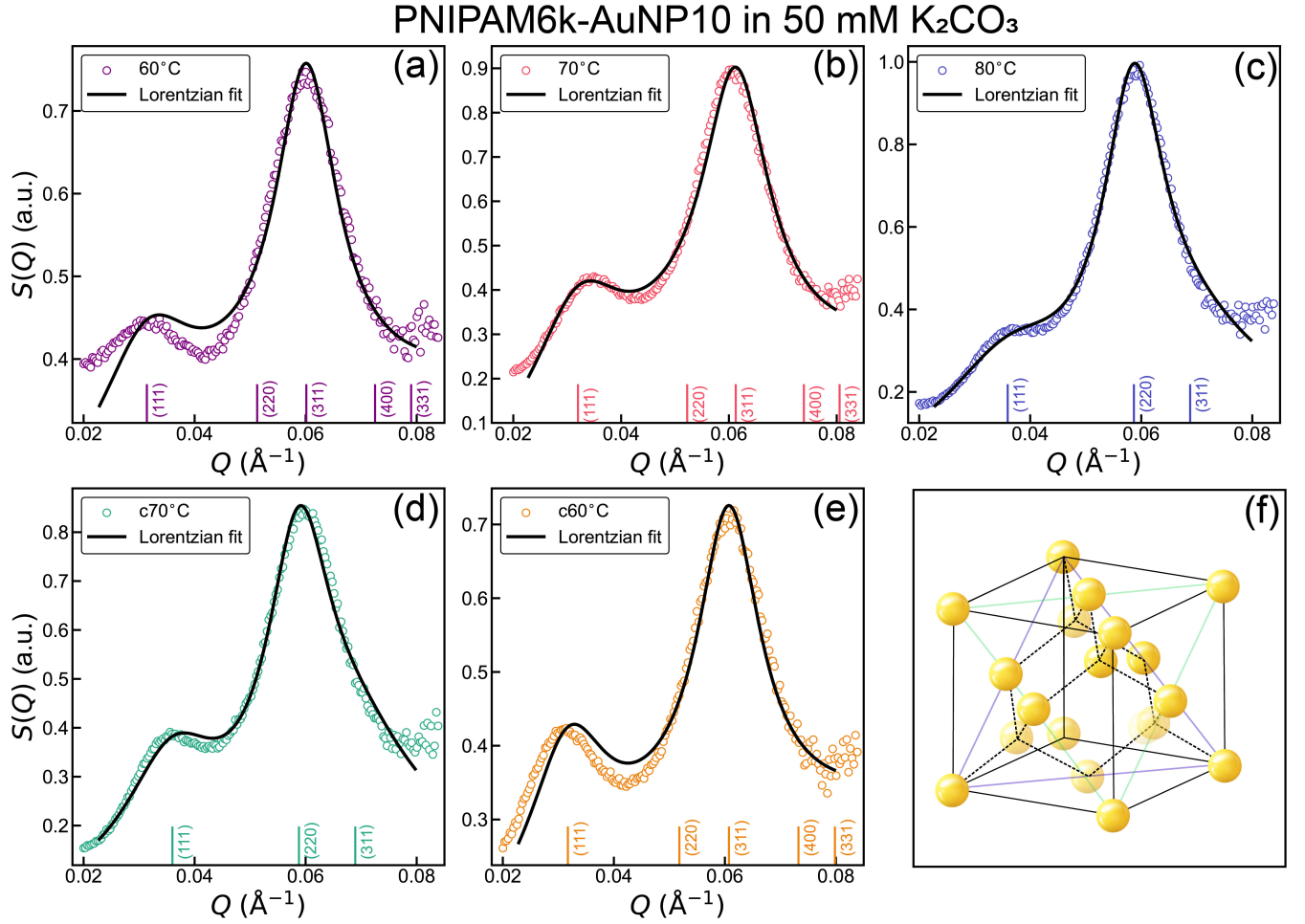


Figure S11: (a-e) Normalized $S(Q)$ profiles of PNIPAM6k-AuNPs in 50 mM K_2CO_3 across various temperatures as indicated. The solid lines represent fits using Lorentzian-shaped functions based on a diamond-cubic lattice model. Vertical lines mark peak positions with their respective Miller indices. Temperatures with a preceding 'c' denote cooling conditions. For clarity, plots have been vertically shifted. (f) Schematic illustration of a simple diamond-cubic lattice.

Table S3: Fitting parameters extracted from Lorentzian functions for the diamond-like cubic lattice of PNIPAM6k-AuNP10 at 50 mM K_2CO_3 under different temperature conditions.

(h, k, l)	60 °C			70 °C			80 °C		
	Q_{hkl} (\AA^{-1})	Intensity (a.u.)	FWHM (\AA^{-1})	Q_{hkl} (\AA^{-1})	Intensity (a.u.)	FWHM (\AA^{-1})	Q_{hkl} (\AA^{-1})	Intensity (a.u.)	FWHM (\AA^{-1})
(1,1,1)	0.0314	4.3	0.0213	0.0324	4.3	0.0212	0.0359	4.3	0.0291
(2,2,0)	0.0512	4.5	0.0505	0.0529	4.5	0.0445	0.0586	6.5	0.0132
(3,1,1)	0.0601	6.4	0.0134	0.0619	6.4	0.0149	0.0688	5.0	0.0350

2D XRR and GISAXS data

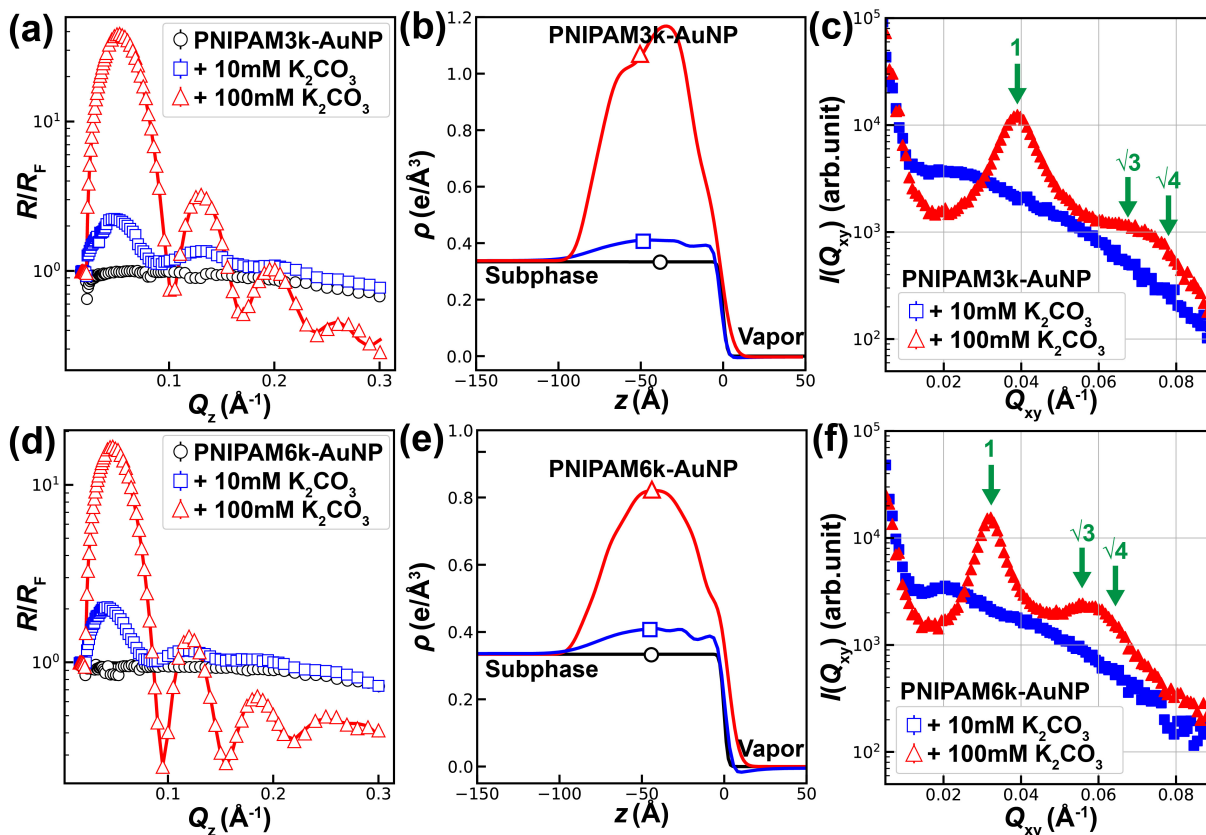


Figure S12: R/R_F data for (a) PNIPAM3k-AuNP and (d) PNIPAM6k-AuNP with increasing K_2CO_3 concentrations. Solid lines of R/R_F data in (a) and (d) are acquired from the best-fit electron density profiles in (b) and (e), respectively. 2D GISAXS data for (c) PNIPAM3k-AuNP and (f) PNIPAM6k-AuNP with increasing K_2CO_3 concentrations. Arrows in (c) and (f) indicate the calculated Q_{xy} positions for a 2D hexagonal lattice.

Figure S12 shows X-ray reflectivity (XRR) and grazing-incidence small-angle X-ray scattering (GISAXS) data from thin films of PNIPAM3k and PNIPAM6k grafted AuNPs at room temperature with various salt concentrations as indicated. The analysis of XRR in terms of ED profiles is shown in Figure S12 (b) and (e). The broad bell-shaped peaks in the ED profiles are due to the AuNP cores. The diffraction pattern in Figure S12 (c) and (f) show broad peaks corresponding to 2D short-range ordering where peak positions at Q values are similar to that are in bulk.

Calculation of grafting density

To determine the grafting density of PNIPAM on the AuNPs, we consider the scenario where PNIPAM3k-AuNPs have completely collapsed, releasing any trapped water. In this state, the overall diameter of the combined nanoparticle closely aligns with d_{NN} . By measuring the difference in volume (ΔV) between the bare AuNP (D calculated from form factor measurements) and this combined structure, we can deduce the volume occupied by the grafted PNIPAM. This, in turn, can be employed to compute the weight of the attached PNIPAM (W_{PNIPAM}) and, subsequently, the number of grafted chains per AuNP.

$$\Delta V = \frac{\pi}{6}(d_{\text{NN}}^3 - D^3) \quad (\text{S1})$$

Weight of PNIPAM:

$$W_{\text{PNIPAM}} = \Delta V \times \rho_{\text{PNIPAM}} \quad (\text{S2})$$

$$\text{Number of chains} = \frac{W_{\text{PNIPAM}}}{MW_{\text{PNIPAM}}} \quad (\text{S3})$$

Where MW is the molecular weight of one PNIPAM chain.

Calculation for PNIPAM3k-AuNPs: $d_{\text{NN}} = 9.68$ nm, $D = 8.7$ nm, $\rho_{\text{PNIPAM}} = 1.1 \frac{\text{g}}{\text{cm}^3}$, $MW = 4.9816 \times 10^{-21}$ g. Substituting these values to Equations S1, S2, S3, we can estimate the number of chains grafted approximately equal to 28.78.

Calculation for PNIPAM6k-AuNPs: $d_{\text{NN}} = 16.75$ nm, $D = 8.6$ nm, $\rho_{\text{PNIPAM}} = 1.1 \frac{\text{g}}{\text{cm}^3}$, $MW = 9.9632 \times 10^{-21}$ g. Substituting these values to Equations S1, S2, S3, we can estimate the number of chains grafted approximately equal to 235.15. Which is higher in number, indicating that it is not in a completely collapsed state with absorbed water.

Calculation of nanoparticle molarity

The molarity of AuNP suspensions is determined using the concentration data provided by the vendor (TedPella Inc.), which specifies the number of particles in a milliliter of solution. This calculation employs the following equation.

$$\text{Molarity (M)} = \frac{\text{Number of particles per ml}}{N_{\text{A}} \times 10^{-3} \text{ liters}} \quad (\text{S4})$$

Where N_{A} is Avogadro's number.

For example, the molarity of 10 nm-sized bare AuNPs is calculated from the particle concentration provided on the vendor technical data sheet (in this case 5.7×10^{12} particles/ml). Using equation S4 yields of 9.46×10^{-9} M, equivalent to 9.46 nM. Upon determining the molarity of the bare AuNPs, UV-visible spectrophotometry is used to ascertain their absorbance at 525 nm wavelength. Assuming the grafting does not affect the signal and aggregation does not occur, by comparing the absorbance profiles of the PNIPAM grafted AuNPs with those of the bare AuNPs, the concentration of the grafted AuNPs in suspension can be determined.